RSC Advances

PAPER

View Article Online
View Journal | View Issue

Cite this: *RSC Adv.*, 2017, **7**, 11149

Temperature-sensitive carbon dots derived from poly(*N*-isopropylacrylamide) for fluorescence on–off properties†

Zihnil Adha Islamy Mazrad,‡[a] Eun Bi Kang,‡[b] Nuraeni,[a] Gibaek Lee,[b] Insik In*[ac] and Sung Young Park*[ab]

Here, we report novel thermo-responsive fluorescent nanoparticles of carbonized poly(*N*-isopropylacrylamide) (PNIPAAm) through two pathways, partial carbonized PNIPAAm (F-PNIPAAm) and full carbonized PNIPAAm (FNP) acid treatment. The carbonized PNIPAAm generated different properties depending on acid treatment time to control the lower critical solution temperature (LCST) behaviors as a biosensor based on a fluorescence on–off system. Furthermore, the FNP–PNIPAAm also showed reversible capability based on fluorescence intensity, with a high fluorescence signal observed at room temperature (25 °C) but quenching at physiological temperature (37 °C). H-NMR, FT-IR, X-ray dispersion (XRD), and X-ray photoelectron spectroscopy (XPS) confirmed the associated chemical moieties of FNP–PNIPAAm and FNP. After confirming the cytotoxicity of the prepared material, we carried out *in vitro* bio-imaging studies using MDAMB, A-549, and MDCK cells by confocal laser-scanning microscopy. Therefore, we successfully established a convenient, rapid, and ecofriendly synthetic approach to the synthesis of FNPs based on PNIPAAm. These FNPs exhibited tunable luminescence properties, high aqueous stability, and low cytotoxicity, suggesting potential applications in bio-labeling, bio-imaging, and optoelectronics.

Received 12th October 2016
Accepted 6th February 2017

DOI: 10.1039/c6ra25104h

rsc.li/rsc-advances

1. Introduction

Fluorescent nanoparticles (FNPs) have recently become widely studied in life sciences due to their tiny size, excellent photoluminescence properties, and high biocompatibility.[1,2] As a new class of fluorescent materials, FNPs have been studied extensively for the development of applications in electronics, light-emitting devices, photocatalysis, and sensors.[3–7] Additionally, because of their low toxicity and the use of environmentally friendly materials, FNPs have also been used for bio-imaging and drug delivery systems.[8–12] Many materials have been used for the synthesis of FNPs, such as graphite, candle soot, and biological sources, such as mango, soy milk, polysaccharides, and plant leaves.[13–18] These FNPs have been successfully manufactured by top-down and bottom-up routes and have been shown to have unique chemical and optical properties with tunable sensitivity and stability for biosensor and bio-imaging probes.[19]

Recently, fluorescent agent-based thermo-responsive materials resulted big attention in wide range of areas because of their potential applications. These studies have demonstrated sensitive and reversible thermo-stimulus for fluorescence-color/on–off switching characteristics, and the fluorescence parameters (intensity, wavelength, and lifetime) showed high sensitivity and linearity depending on the temperature. This approach have been found within biomedical uses, including the release of drugs at body temperature as a common method in thermo-responsive studies, and their use in biomedical applications will have a definite impact in the medical field.[20] Poly(*N*-isopropylacrylamide) (PNIPAAm) is a well-known temperature-sensitive linear polymer that exhibits a lower critical solution temperature (LCST) of approximately 32 °C in aqueous solution, becoming less soluble and coagulating at temperatures higher than 32 °C to form a hydrophobic material.[21] Considering all of these advantages, PNIPAAm play an important role in biomedical applications such as in drug delivery systems, controlled release of drugs, and tissue engineering.[22–24] Moreover, the PNIPAAm chain consists of abundant amounts of carbon, nitrogen, and oxygen, leading to possess fluorescent properties through the acid treatment owing to simultaneous partial carbonization and thereby affecting LCST behaviors in the context of increased temperatures.

Inspired from thermo-sensitive PNIPAAm and the electronic response of carbonized material, we aimed to create new desirable agents possessing the capacity for application as a fluorescence on–off biosensor and bioimaging agent.[14]

[a]*Department of IT Convergence, Korea National University of Transportation, Chungju 380-702, Republic of Korea. E-mail: parkchem@ut.ac.kr*

[b]*Department of Chemical and Biological Engineering, Korea National University of Transportation, Chungju 380-702, Republic of Korea*

[c]*Department of Polymer Science and Engineering, Korea National University of Transportation, Chungju 380-702, Republic of Korea*

† Electronic supplementary information (ESI) available. See DOI: 10.1039/c6ra25104h

‡ These authors equally contributed to this work.

Generally, PNIPAAm does not show photoluminescence behavior during excitation; however, after acid treatment, carbonized PNIPAAm exhibits bright blue fluorescence due to surface functionalization by carboxylic acid or amine groups in the NIPAAm chain. PNIPAAm has been extensively studied as a thermoresponsive polymer that acts as a reversible switch between hydrophilic and hydrophobic states in response to temperature change. This polymer exhibits an LCST that undergoes a phase transition at 32 °C in aqueous solution.[22–25] Moreover, PNIPAAm transforms from the water-swollen state to the globular state when heated to above its LCST in aqueous solution.

In this work, we prepared two materials by controlling the carbonization times of PNIPAAm to obtain thermo sensitive fluorescent nanoparticles. We then attempted to establish a simple, low-cost strategy for the synthesis of temperature-sensitive FNPs prepared using PNIPAAm as a precursor material with a defined dehydrating system to control the time of the reaction. Carbonization was carried out for 1 min or 1 h using two different acid treatments, confirming that the treatment will help to maintain LCST behaviors of PNIPAAm. These carbonized nanoparticles produced a bright blue fluorescence with good solubility in water, could be effectively served in bio-labeling, bio-imaging, and optoelectronics.

2. Experimental

2.1 Materials and experimental procedures

N-Isopropylacrylamide (NIPAAm), 2-mercaptoethanol (≥99.0%), 2,2′-azobis(2-methylpropionitrile; 98%; AIBN), sulfuric acid (H_2SO_4, 95%), and sodium hydroxide (NaOH) were purchased from Sigma Aldrich (Korea). MDAMB-231, A549, and MDCK cells were obtained from Korean Cell Line Bank (Seoul, Korea). Penicillin–streptomycin, phosphate-buffered saline (PBS), 0.05% (w/v) trypsin EDTA (1×) solution, and RPMI-1640 medium were purchased from Gibco BRL (Carlsbad, CA, USA). Particle sizes were examined using dynamic light scattering (DLS; Zetasizer Nano, lvern Germany). The absorbance and fluorescence were monitored by UV-visible spectroscopy (Optizen 2120 UV; Mecasys Co. Ltd.) and fluorescence spectroscopy (FluoroMate; Scinco Co. Ltd., Korea), respectively. Transmission electron microscopy (TEM) images were taken on a TECNAI F20 (Philips) at 200 kV, and the elemental compositions were determined by X-ray photoelectron spectroscopy (XPS) using an Omicrometer ESCALAB (Omicrometer, Taunusstein, Germany). The confocal images of cells were obtained using an LSM510 confocal laser-scanning microscope (CLSM; Carl Zeiss, Germany) equipped with a 364 nm UV laser and 543 nm He/Ne laser. Raman spectra was observed using Fourier transform Raman (FT-Raman, RFS 100/S FT-Raman spectrophotometer, Bruker, Fahrenheitstr, 4 D-28359 Bremen, Germany). PNIPAAm (M_n: 22 600) was prepared as previously described.[21]

2.2 Preparation of fluorescent carbon nanoparticles (FNP–PNIPAAm and FNPs) from PNIPAAm

To prepare thermosensitive FNP–PNIPAAm, 1.0 g of PNIPAAm was added to 10 mL of concentrated H_2SO_4 and mixed with bar stirrer. The reaction was then carried for 1 min for FNP–PNIPAAm and 1 h for FNP. Finally, FNP–PNIPAAm and FNPs were collected, followed by neutralization with NaOH (1 M), dialysis (1000 Da molecular weight cut off [MWCO]), and freeze drying.

2.3 Cytotoxicity assay

For *in vitro* cytotoxicity, MDAMB-231, A549, and MDCK cells were cultured in RPMI medium supplemented with 10% fetal bovine serum (FBS), 100 U mL^{-1} penicillin, and 100 μg mL^{-1} streptomycin. The cells were then incubated for 1 day in a humidified atmosphere containing 5% CO_2 at 37 °C for 3 days. The cytotoxicity of the cells was measured using 3-(4,5-dimethylthiazol-2-yl)-2,5-diphenyltetrazolium bromide (MTT) assays. Briefly, 200 μL of cells at a density of 2×10^5 cells per well were placed into each well of a 96-well plate then incubated for next 24 h at 37 °C. Next, the medium was removed, and the cells were incubated with different concentrations of FNP–PNIPAAm and FNPs ranging from 0.001 to 1 mg mL^{-1}. Cells were added alone as a blank control. The cells were then incubated as described above for another 24 h. The medium containing the samples were then removed, after which the cells was washed with PBS and added 200 μL of a stock solution containing 2 mg mL^{-1} MTT in PBS. Cells were incubated for another 4 h, and 180 μL MTT solubilizing agent was added to the cells. Cells were shaken for 15 min, and absorbance was measured at a wavelength of 570 nm using microplate reader (Varioskan Flash, Thermo Electron Corporation). The relative cell viability was measured by comparing with control wells containing cells alone.

2.4 *In vitro* imaging and evaluation of cellular uptake

Using the cells described above, we carried out *in vitro* imaging. A total of 5×10^5 cells per well was plated in 8-well plates. All cells were treated with the same concentration (0.1 mg mL^{-1}) of FNP–PNIPAAm and FNP then incubated for 2 h at 37 °C in a humidified atmosphere containing 5% CO_2. Finally, the cells were washed with PBS several times, and fresh culture medium was added. The cells were imaged using an LSM510 CLSM (Carl Zeiss). For the prepared samples, excitation was carried out at 488 nm with an emission filter of 455 nm and 505 nm. During all investigations, the objective lens was 20×.

3. Results and discussion

A potential scheme for the synthesis of FNP–PNIPAAm and FNP from PNIPAAm as potential thermoresponsive FNPs is shown in Scheme 1. Thermo-responsive FNPs were obtained by treating with sulfuric acid (H_2SO_4) at controlled temperature and time for the functionalization of PNIPAAm. The reaction was carried out at two conditions: complete and partial carbonization. The differences in the molecular structures of the treated polymers were characterized by ^{1}H-nuclear magnetic resonance (NMR) and Fourier transform-infrared (FT-IR) spectroscopy, as shown in Fig. 1. The ^{1}H NMR spectrum contained peaks at 3.6 and 4.0 ppm (Fig. 1a), which were assigned to (CH–) and (–CH_2–) peaks of the PNIPAAm chains, and two main characteristic

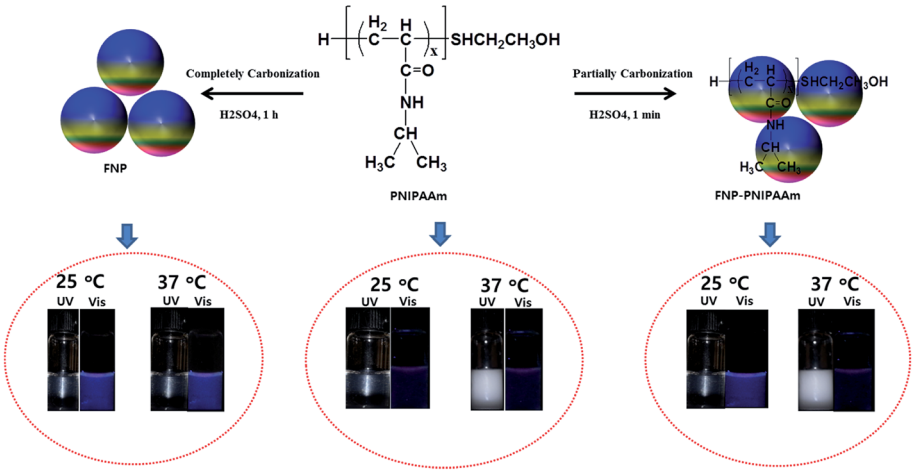

Scheme 1 Synthesis routes of prepared FNP and FNP–PNIPAAm as thermoresponsive biosensor.

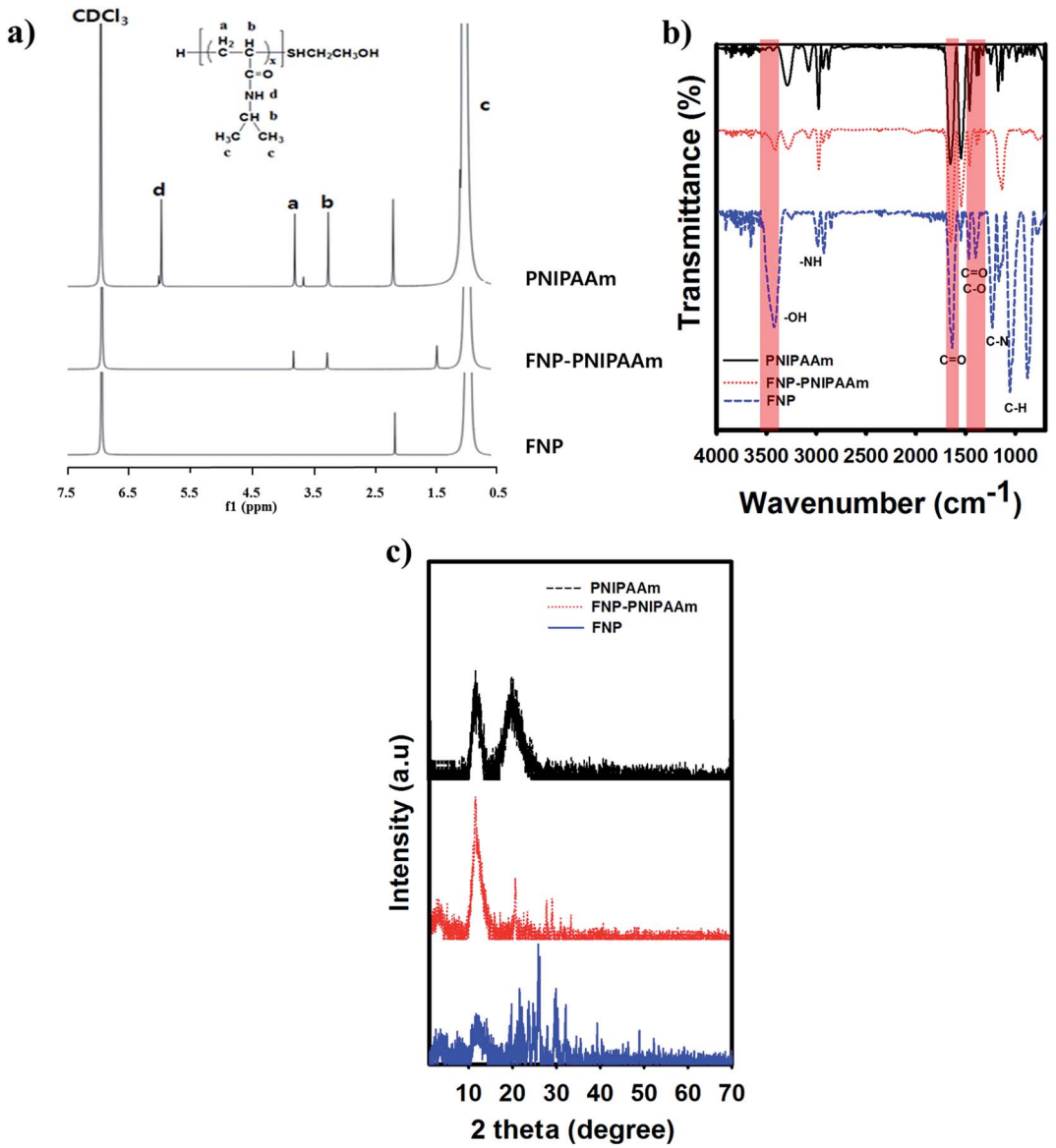

Fig. 1 ^{1}H-NMR (a) and FTIR (b) spectra of PNIPAAm, FNP–PNIPAAm, and FNP (c) the X-ray diffraction (XRD) patterns in the range of 1 to 80° for PNIPAAm, FNP–PNIPAAm, and FNP.

peaks at 6.2 and 1.0 ppm, which were attributed to the –NH– and $–CH_3$ moieties, respectively.[26] However, the (CH–) and ($–CH_2–$) peaks in ^{1}H-NMR spectra were found to be absent from FNP because of the complete acid treatment. Moreover, FT-IR spectra (Fig. 1b) demonstrated the presence of hydroxyl groups (3400 cm^{-1}) of acid-treated PNIPAAm. In addition to this peak, we also observed N–H stretching and C=O stretching vibration peaks at 3225 and 1700 cm^{-1}, respectively, suggestive of the appearance of amine and carboxyl linkages of FNP–PNIPAAm.[27,28] In X-ray diffraction (XRD) patterns as shown in Fig. 1c, unmodified PNIPAAm shows a primary crystalline peak centered at around $2\theta = 20°$, including an amorphous peak at $2\theta = 12°$. After hydrothermal treatment, the intensity of the amorphous peak was increased by reducing the crystalline peak, indicating that the PNIPAAm was partially oxidized into FNP–PNIPAAm, while the FNP amorphous peak was observed at around $2\theta = 20–40°$, confirming the complete carbonization after prolonged acid treatment.[29] Fig. S1† show Raman studies of PNIPAAm partial and complete acid treatment, indicating the presence of peak at area 1370 nm as D band and 1540 nm as G band. G/D bands imply sp^3 and sp^2 carbon contents, which is used to correlate different ratios of the sp^2/sp^3 to understand the existence of defects in the carbonized material.[29] Regarding the G/D band peaks, we conclude full carbonization of PNIPAAm gives rise content of sp^2, implying more defect compared with partially carbonized PNIPAAm.

To evaluate the thermo-responsive nature of FNP–PNIPAAm and FNP, we observed their absorption properties using UV-Vis spectroscopy at three temperatures (25, 30 and 37 °C). The UV-Vis spectra exhibited an absorbance peak at 300 nm (Fig. 2a and b), which referred to as the $\pi–\pi^*$ transition of the carbon bond derived from the PNIPAAm polymer chain.[30] Fig. 2a shows the absorption curve of FNP–PNIPAAm increased with enhancement temperature because of the reducing transmittance of sample, implication soluble-to-insoluble phase transition in an aqueous medium at around 37 °C, which was not observed of the FNP. To compare the LCST behaviors (Fig. 2c) of our samples, we observed FNP–PNIPAAm and FNP behavior at 20 to 60 °C. The FNP–PNIPAAm produced the same LCST behavior about 30 °C as PNIPAAm, whereas fully carbonized FNP did not show the same behaviors owing to disappearance of the natural structure of the NIPAAm unit. These data clearly confirmed that after acid treatment of FNP–PNIPAAm for 1 min, some partial carbonized PNIPAAm was present, which helped to maintain the LCST behaviors for further applications.

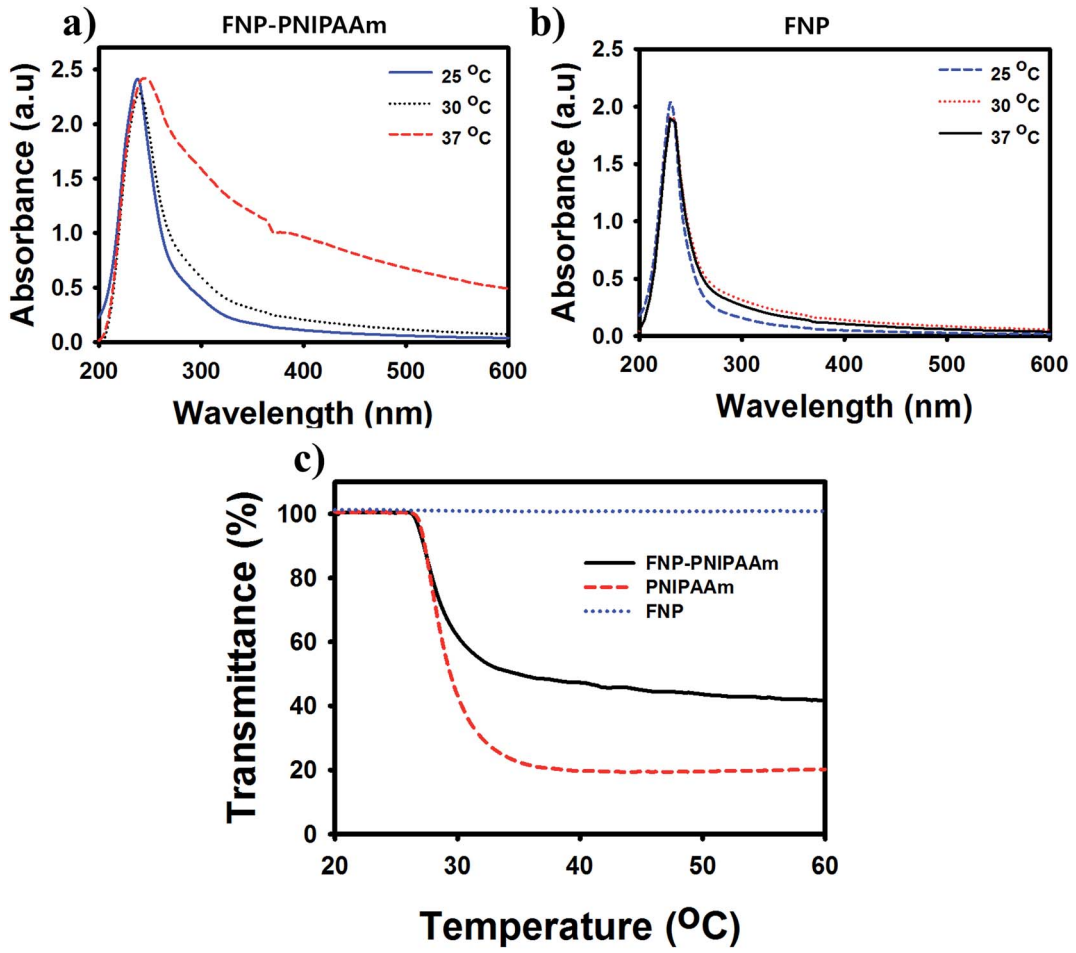

Fig. 2 UV-Vis spectra of FNP–PNIPAAm (a) and FNP (b) at different temperatures. (c) LCST behaviors of PNIPAAm, FNP–PNIPAAm, and FNP at 20–60 °C.

Carbonized materials usually contain a mixture of sp^2 type π bonding and the light emission from such carbon system are a consequence of the geminate recombination of localized electron–hole (e–h) pairs in sp^2 clusters, which essentially behave as luminescence centers or chromophores. Although the emission energy bandgap depends on the size, shape, and fraction of the sp^2 domains, tunable light emission can be achieved by controlling the nature of carbonization.[31] These carbonized PNIPAAm molecules showed fluorescence behaviors due to a quantum effect including different emissive traps on the surface of FNP.[32] To confirm the photoluminescence (PL) properties of FNP–PNIPAAm, we first performed experiments under a UV lamp at 365 nm, observing blue fluorescence emission. By evaluating the PL spectra of FNP–PNIPAAm, we found that the highest emission intensity was centered at 385 nm when the excitation energy was 340 nm (Fig. 3). Furthermore, as shown in Fig. 3a, we analyzed the effects of room temperature and physiological temperature for FNP–PNIPAAm; higher fluorescence emission was observed at room temperature, and there was no detectable fluorescence found at physiological temperature. The quenching mechanism of the FNP–PNIPAAm, which was not observed for FNP (Fig. 3b), could be attributed to the formation of micelle nanoparticles *via* hydrophilic and hydrophobic interactions maintained by partial carbonizing of PNIPAAm at high temperature; however, at room temperature, no fluorescence off signal occurred, which could be attributed to the hydrophilic nature of the NIPAAm unit.[33] In addition, we have investigated the study to obtain the carbonized PNIPAAm dependent on different acid treatment time (10–50 min). Fig S2a† shows slightly increase dependent on increasing reaction time. Otherwise after increase the temperature (37 °C), a quenching was not seen at 50 min treatment due to the losing of NIPAAm structure effect by fully carbonized treatment (Fig. S2b†). Furthermore, Fig. S3† represent the fluorescent behavior of the partial carbonized PNIPAAm observed at 10–50 °C to understand the effect of temperature range. The sharp quenching effect has start at 40 °C whereas at 10–30 °C there is no clearly fluorescence changes were observed, it means the effect to fluorescence related to LCST value of PNIPAAm. This mechanism provides a responsiveness that may be useful for temperature-triggered detection of tumor cells. The reversible temperature-triggered behavior shown in Fig. 3c was confirmed through three cycles of reversible fluorescence quenching achieved by adjusting the temperature from 25 to 37 °C. The fluorescence remained stable as the temperature changed through several cycles, indicating the thermostability of FNP–PNIPAAm.

The DLS data also showed that the diameter increased as the temperature increased because of coagulation, confirming the existence of PNIPAAm properties after acid treatment in FNP–PNIPAAm (Fig. 4a and b). In contrast, fully carbonized FNP showed almost the same particle sizes as the temperature

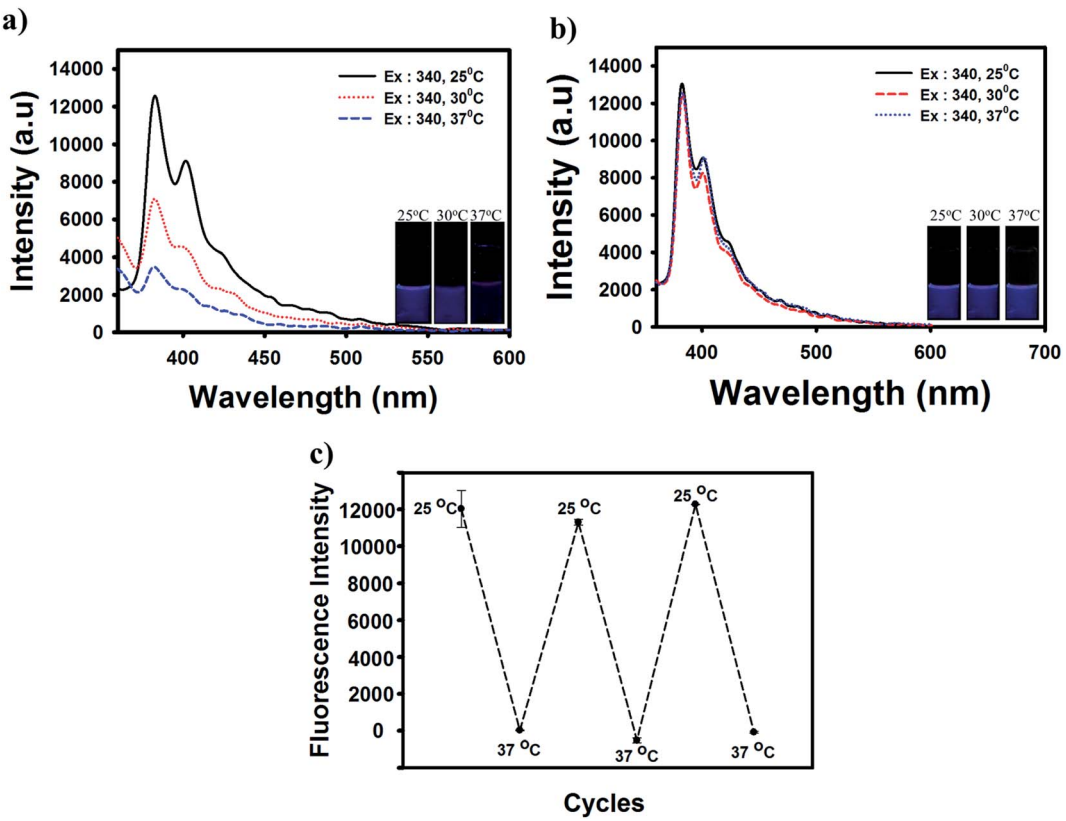

Fig. 3 The fluorescence emission spectra of FNP–PNIPAAm (a) and FNP (b) at different temperatures with fixed excitation at 340 nm. (c) Reversible behaviors of FNP–PNIPAAm upon cycling the temperature between 25 and 37 °C at a maximum emission wavelength when excited at 340 nm.

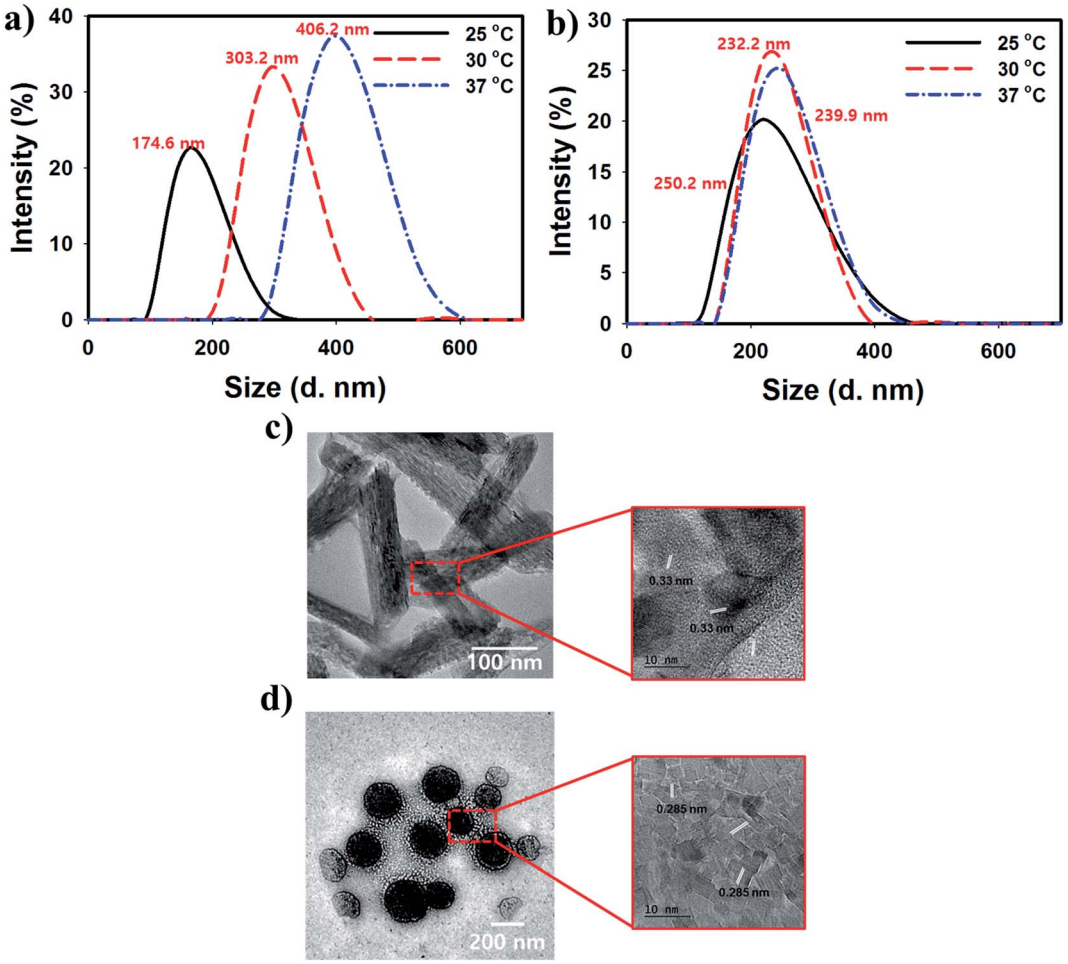

Fig. 4 Dynamic light spectroscopy (DLS) of FNP–PNIPAAm (a) and FNP (b) at different temperatures. TEM images of (c) FNP–PNIPAAm and (d) FNP.

increased, implying loss of the thermosensitivity of PNIPAAm. TEM images of FNP–PNIPAAm (Fig. 4c) showed cylinder-shaped particles with small defects and a comparatively narrow size distribution (150–200 nm) because the short carbonizing time preserved the PNIPAAm shape after acid treatment (Fig. S4†). In contrast, FNP (Fig. 4d) were dot shaped after full acid treatment, with the lattice separations of those carbonized materials (~0.285–0.33 nm), confirming the presence of graphene carbon structures indicative of internalized carbon particles.[34]

The survey scans of XPS results were also consistent with the FT-IR analysis. Based on the XPS analysis (Fig. 5a), the as-prepared acid-treated PNIPAAm and FNP contained a high percentage of oxygen atoms compared with PNIPAAm because of the functionalization of carboxylic or amine groups in the FNP–PNIPAAm chain. Next, the C1s core level spectrum of FNP–PNIPAAm and FNP showed a considerable degree of oxidation with four components corresponding to carbon atoms with different functional groups, *i.e.*, oxygenated C (C=O) at 287.5–292 eV, C–C bonds (284.5 eV), C=C bonds (284 eV), and C–N bonds (285.4 eV), and a prominent π–π^* transition peak appeared at 292 eV, showing the presence of some carboxylic and hydroxyl groups on the carbonized FNP.[14] Fig. 5b shows the elemental composition of PNIPAAM, FNP–PNIPAAm, and FNP in C1s analysis; the results showed increased percentages of sp^2-type carbons in FNP.

To visualize the fluorescence state in cell, we used confocal images of FNP–PNIPAAm and FNP monitored with a CLSM (Fig. 6a), which can be used for cellular imaging and diagnosis. For fluorescence microscopic images, the corresponding cells were loaded with both bioimaging agents, showing emission of blue and green fluorescence after 4 h of incubation after excitation with their corresponding excitation wavelength. Notably, the nanoparticles were accumulated within the cell cytoplasm randomly owing to nonspecific delivery of FNPs. The results from confocal images support the use of these agents as strong candidates for cellular imaging and diagnosis. To evaluate the cytotoxic behavior of FNP–PNIPAAm, we examined the *in vitro* cytotoxicity in three cell types, including MDAMB, A549, and MDCK cells. Our findings confirmed that this material was not toxic, with ~100% cell viability observed after treatment with FNP–PNIPAAm at different concentrations. Similar results were observed for FNP. Thus, these materials may be applied as nontoxic material for biological purposes (Fig. 6b and S5†).[35]

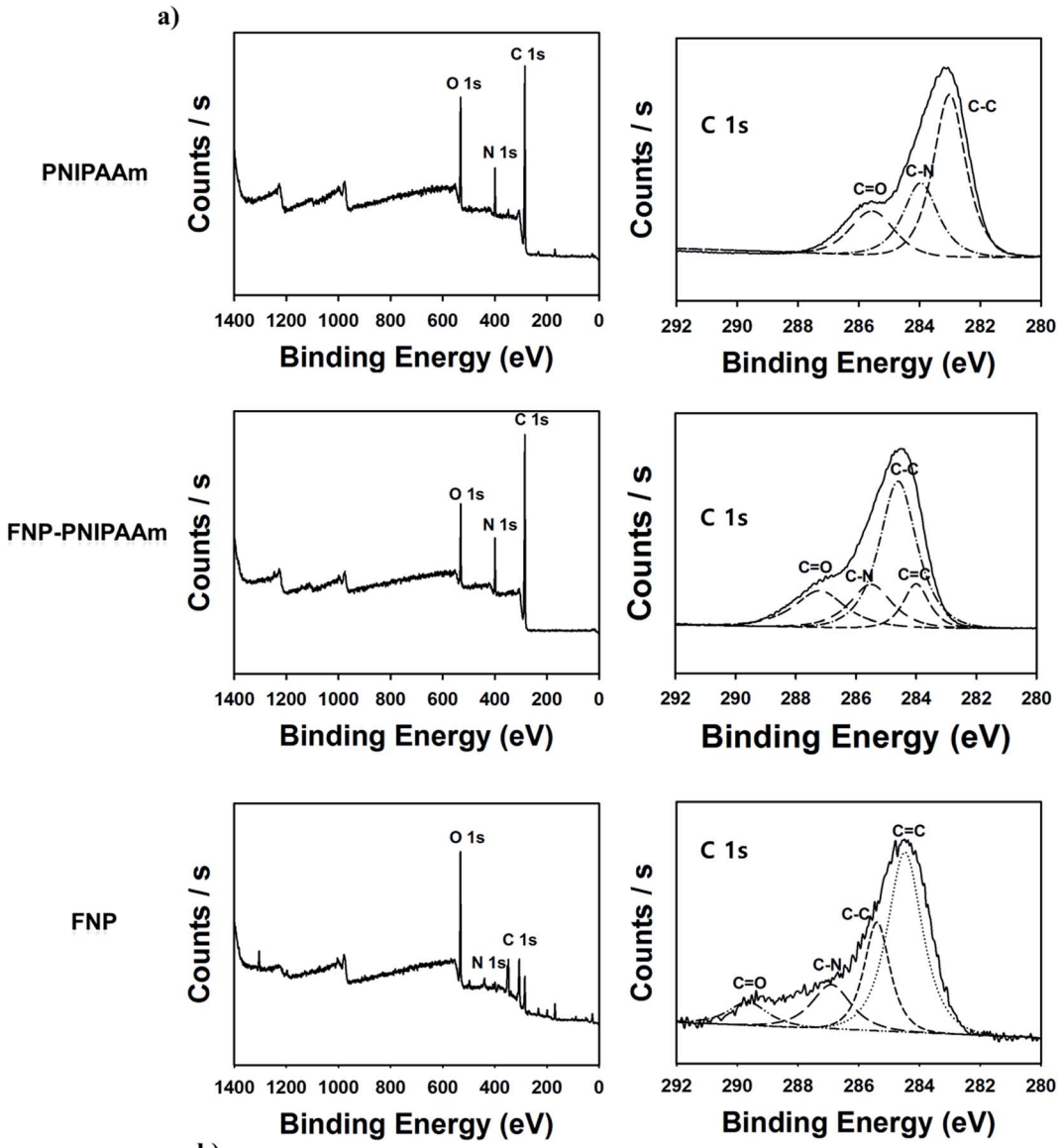

b)

PNIPAAm	Area (%)	FNP-PNIPAAm	Area (%)	FNP	Area (%)
C=O	17.52	C=O	18.04	C=O	14.99
C-C	64.07	C-C	53.31	C-C	28.01
C-N	18.41	C-N	17.57	C-N	17.78
C=C	-	C=C	11.08	C=C	39.12
ratio (sp2/sp3)	1/0	ratio (sp2/sp3)	1/0.21	ratio (sp2/sp3)	1/1.39

Fig. 5 (a) Survey scan of PNIPAAm, FNP–PNIPAAm, and FNP, deconvoluted C1s peak of PNIPAAM, FNP–PNIPAAm and FNP. (b) XPS-based elemental carbon (C1s) analysis of PNIPAAm, FNP–PNIPAAm, and FNP.

This work can control the fluorescent behavior through carbonization time and obtain the reversible behavior by temperature change based on PNIPAAm and thermoresponsive polymer. Some studies reported that unique fluorescent properties can be from graphene carbon nanodots treated by ultrasonication, which generate visible emission with near-infrared

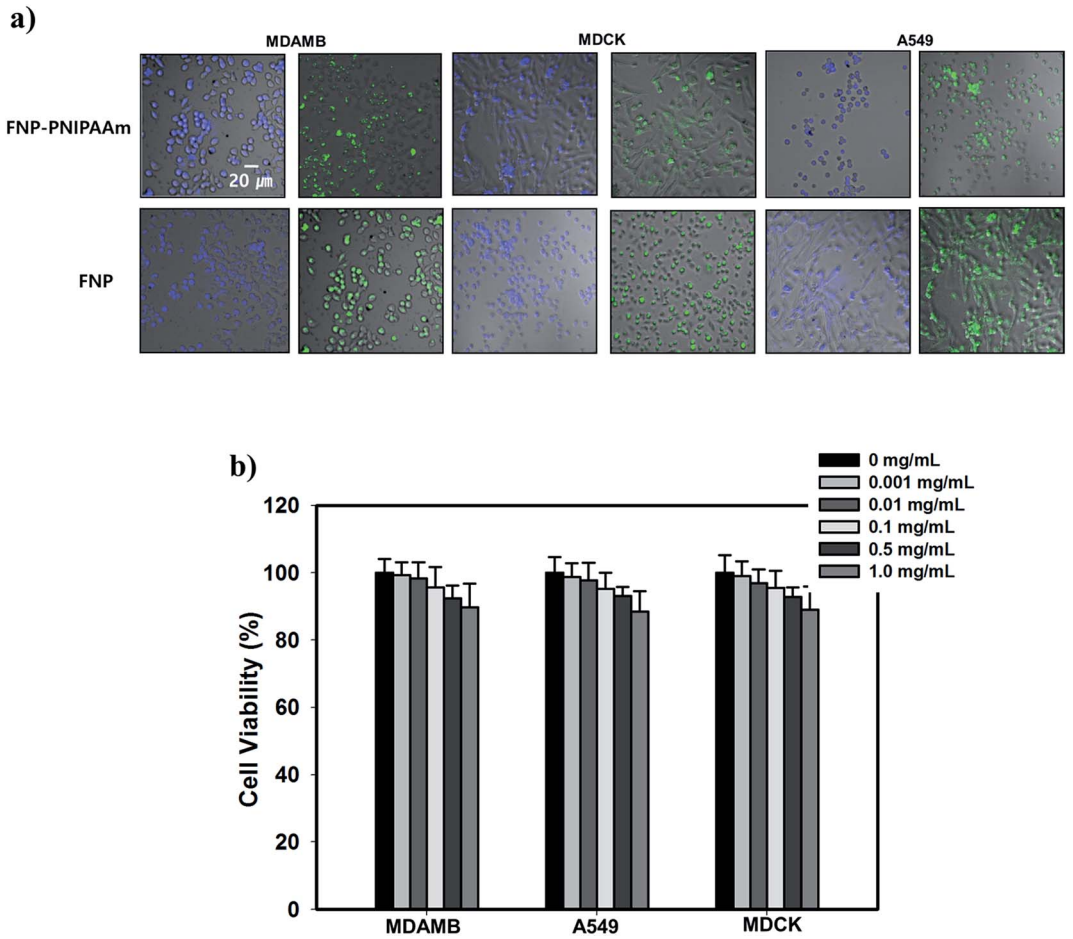

Fig. 6 (a) Confocal microscope images of MDAMB, A549, and MDCK cells treated with FNP–PNIPAAm and FNP observed during a 4 h incubation period at 455 and 504 nm. (b) Cell viability of FNP–PNIPAAm after a 24 h incubation using MDAMB, A549, and MDCK cells.

(NIR) excitation.[36] But this FNPs based carbonized PNIPAAm showed intrinsic emission which can quench based LCST behavior dependent on carbonization time, resulting reversible fluorescent on/off system based temperature change.

4. Conclusions

In conclusion, we firstly established a convenient, rapid, and eco-friendly synthetic approach for the synthesis of thermosensitive FNPs based on the PNIPAAm polymer. The fluorescent system was prepared using two pathways, partially carbonized FNP–PNIPAAm and fully carbonized FNP; these materials exhibited strong blue fluorescent emission without further surface treatment. We can control the temperature-responsive behaviors of FNPs by modifying the carbonization time; indeed, after 1 h of acid treatment, the FNP lost their LCST behavior. H-NMR, FT-IR, XRD, and XPS spectroscopy confirmed the associated chemical moieties of FNP–PNIPAAm and FNP, which had high percentages of sp^2 groups. The FNP–PNIPAAm showed stable LCST behavior upon cycles of temperature changes, permitting the reversibility of FNP–PNIPAAM as a biosensor. After confirming the cytotoxicity of the prepared material, we carried out *in vitro* bioimaging studies using MDAMB, A-549, and MDCK cells; the results showed that the cells were loaded with bioimaging agents. Because of their temperature-tunable luminescence properties, high aqueous stability and low cytotoxicity, this agent could be effectively served for biolabeling, bioimaging, and optoelectronic applications.

Acknowledgements

This study was supported by Grant No. 10062079, R0005303 and R0005237 from the Ministry of Trade, Industry & Energy (MOTIE), and the Basic Science Research Program through the National Research Foundation of Korea (NRF) funded by the Ministry of Education (No. 2014055946).

References

1 X. Yang, W. Ming, F. Xi-Zeng, Y. Xue-Bo, H. Xi-Wen and Z. Yu-Kui, *Chem.–Eur. J.*, 2013, **19**, 6282–6288.
2 K. Welsher, Z. Liu, S. P. Sherlock, J. T. Robinson, Z. Chen, D. Daranciang and H. Dai, *Nat. Nanotechnol.*, 2009, **4**, 773–780.
3 X. Zhang, Y. Zhang, Y. Wang, S. Kalytchuk, S. W. Kershaw, Y. Wang, P. Wang, T. Zhang, Y. Zhao, H. Zhang, T. Cui,

Y. Wang, J. Zhao, W. W. Yu and A. L. Rogach, *ACS Nano*, 2013, **7**, 11234–11241.
4 M. Peter, J. H. Eric, S. Navid, M. Y. Christopher and A. O. Geoffrey, *J. Mater. Chem.*, 2012, **22**, 1265–1269.
5 Y. K. Kim, S. M. Sharker, I. In and S. Y. Park, *Carbon*, 2016, **103**, 412–416.
6 Y. Hang, Z. Hengchao, H. Hui, L. Yang, L. Haitao, M. Hai and K. Zhenhui, *New J. Chem.*, 2012, **36**, 1031–1035.
7 Z. Li, L. Youhui, H. Zhenzhen, R. Jinsong and Q. Xiaogang, *Chem. Commun.*, 2012, **48**, 3686–3899.
8 S. H. Kim, S. Md. Sharker, H. Lee, I. In and S. Y. Park, *RSC Adv.*, 2016, **6**, 61482–61491.
9 Z. A. Qiao, Y. Wang, Y. Gao, H. Li, T. Dai, Y. Liu and Q. Huo, *Chem. Commun.*, 2010, **46**, 8812–8814.
10 E. B. Kang, J. E. Lee, J. H. Jeong, G. Lee, I. In and S. Y. Park, *J. Ind. Eng. Chem.*, 2016, **33**, 336–340.
11 P. Sunil, T. Mukeshchand, M. Ashmi, A. Dhanashree, M. Neeraja and S. Madhuri, *J. Mater. Chem. B*, 2013, **1**, 4972–4982.
12 W. Qinlong, H. Xiaoxiao, L. Yijuan, W. Ziliang, Z. Haijie, Z. Rui, L. Liping, T. Ping and Z. Huzhi, *Carbon*, 2013, **59**, 192–199.
13 H. Li, X. He, Z. Kang, H. Huang, Y. Liu, J. Liu, S. Lian, C. H. Tsang, X. Yang and S. T. Lee, *Angew. Chem., Int. Ed.*, 2010, **26**, 4430–4434.
14 H. Liu, T. Ye and C. Mao, *Angew. Chem., Int. Ed.*, 2007, **34**, 6473–6475.
15 C. J. Jeong, R. K. Arup, H. K. Sung, J. E. Lee, J. H. Jeong, I. Insik and S. Y. Park, *Nanoscale*, 2014, **6**, 15196–15202.
16 Z. Chengzhou, Z. Junfeng and C. Dong, *Chem. Commun.*, 2012, **48**, 9367–9369.
17 Z. Liangliang, Y. Yongjin, W. Cai-Feng and C. Su, *J. Mater. Chem.*, 2013, **1**, 4925–4932.
18 D. O. Mihir, M. Ramavatar and A. K. Siddhanta, *Carbohydr. Polym.*, 2012, **87**, 1971–1979.
19 D. Lisse, C. P. Richter, C. Drees, O. Birkholz, C. You, E. Rampazzo and J. Piehler, *Nano Lett.*, 2014, **4**, 2189–2195.
20 (*a*) R. Davis, N. P. Rath and S. Das, *Chem. Commun.*, 2004, 74–75; (*b*) X. Zhang, Z. Chi, B. Xu, L. Jiang, X. Zhou, Y. Zhang, S. Liu and J. Xu, *Chem. Commun.*, 2012, **48**, 10895–10897; (*c*) B. Yoon, J. Lee, I. S. Park, S. Jeon, J. Lee and J. M. Kim, *J. Mater. Chem. C*, 2013, **1**, 2388–2403; (*d*) T. Mutai, H. Satou and K. Araki, *Nat. Mater.*, 2005, **4**, 685–687.
21 (*a*) M. Heskins and J. E. Guillet, *J. Macromol. Sci., Chem.*, 1968, **2**, 1441–1455; (*b*) F. Shouei, K. Kubota and I. Ando, *J. Phys. Chem.*, 1989, **93**, 3311–3313.
22 (*a*) G. L. Seung, A. P. Tod, K. Wonsang, F. B. Giuseppe, A. G. William and S. J. Seung, *J. Phys. Chem. C*, 2012, **116**, 15974–15985; (*b*) M. Bathfield, J. Reboul, T. Cacciaguerra, P. L. Desmazes and C. Gerardin, *Chem. Mater.*, 2016, **28**, 3374–3384.
23 B. Wang, X. D. Xu, Z. C. Wang, S. X. Cheng, X. Z. Zhang and R. X. Zhuo, *Colloids Surf., B*, 2008, **64**, 34–41.
24 G. Arijit, P. Abhijit, O. S. Suma and K. S. Kalyan, *Asian J. Pharm. Sci.*, 2015, **10**, 99–107.
25 L. Fan, W. Hong, Z. Hui, L. Fei, G. Chun-hu and Y. Qian, *Carbohydr. Polym.*, 2009, **77**, 773–778.
26 H. Xin, B. Cyrille, P. D. Thomas and B. Volga, *Polym. Chem.*, 2011, **21**, 1505–1512.
27 X. L. Ze, L. W. Zhu, X. G. Ming, L. Hui and Z. H. Cheng, *Chem. Commun.*, 2016, **52**, 2063–2066.
28 Z. L. Wu, P. Zhang, M. X. Gao, C. F. Liu, W. Wang, F. Leng and C. Z. Huang, *J. Mater. Chem. B*, 2013, **1**, 2868–2873.
29 Y. Yang, J. Cui, M. Zheng, C. Hu, S. Tan, Y. Xiao, Q. Yang and Y. Liu, *Chem. Commun.*, 2012, **3**, 380–382.
30 C. H. Pin and T. C. Huan, *Chem. Commun.*, 2012, **48**, 3984–3986.
31 E. Goki, L. Yun-Yue, M. Cecilia, Y. Hisato, C. Hsin-An, C. I-Sheng, C. Chun-Wen and C. Manish, *Adv. Mater.*, 2010, **22**, 505–508.
32 Y. P. Sun, B. Zhou, Y. Lin, W. Wang, K. A. Fernando, P. Pathak, M. J. Meziani, B. A. Harruff, X. Wang, H. Wang, P. G. Luo, H. Yang, M. E. Kose, B. Chen, L. M. Veca and S. Y. Xie, *J. Am. Chem. Soc.*, 2006, **24**, 7756–7757.
33 (*a*) A. Nagai, R. Yoshii, T. Otsuka, K. Kokado and Y. Chujo, *Langmuir*, 2010, **26**, 15644; (*b*) S. Y. Park, H. J. Baik, Y. T. Oh, K. T. Oh, Y. S. Youn and E. S. Lee, *Angew. Chem., Int. Ed.*, 2011, **50**, 1644.
34 X. Yu, H. Fan, Y. Liu, Z. Shi and Z. Jin, *Langmuir*, 2014, **30**, 5497–5505.
35 M. Z. A. Islamy, I. In and S. Y. Park, *RSC Adv.*, 2016, **6**, 54486–54490.
36 A. Ciesielski, S. Haar, A. Aliprandi, M. E. Garah, G. Tregnago, G. F. Cotella, M. E. Gemayel, F. Richard, H. Sun, F. Cacialli, F. Bonaccorso and P. Samorì, *ACS Nano*, 2016, **10**, 10768–10777.